Solving the Thermoelectric Trade-Off Problem with Metallic Carbon **Nanotubes**

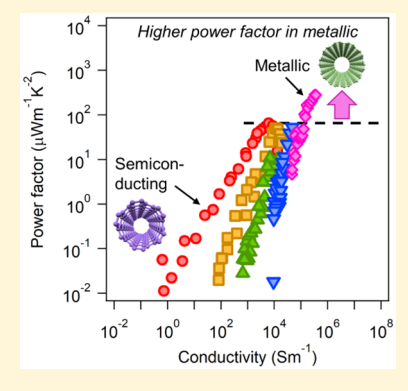
Yota Ichinose,[†] Akari Yoshida,[†] Kanako Horiuchi,[†] Kengo Fukuhara,[†] Natsumi Komatsu,[‡] Weilu Gao,[‡] Yohei Yomogida, ** Manaho Matsubara, ** Takahiro Yamamoto, ** Junichiro Kono, **,‡,||,⊥| and Kazuhiro Yanagi*,†®

Supporting Information

See https://pubs.acs.org/sharingguidelines for options on how to legitimately share published articles.

Downloaded via RICE UNIV on June 30, 2020 at 17:19:30 (UTC).

ABSTRACT: Semiconductors are generally considered far superior to metals as thermoelectric materials because of their much larger Seebeck coefficients (S). However, a maximum value of S in a semiconductor is normally accompanied by a minuscule electrical conductivity (σ), and hence, the thermoelectric power factor ($P = S^2 \sigma$) remains small. An attempt to increase σ by increasing the Fermi energy $(E_{\rm F})$, on the other hand, decreases S. This trade-off between S and σ is a well-known dilemma in developing high-performance thermoelectric devices based on semiconductors. Here, we show that the use of metallic carbon nanotubes (CNTs) with tunable E_F solves this long-standing problem, demonstrating a higher thermoelectric performance than semiconducting CNTs. We studied the $E_{\rm F}$ dependence of S, σ , and P in a series of CNT films with systematically varied metallic CNT contents. In purely metallic CNT films, both S and σ monotonically increased with $E_{\rm F}$, continuously boosting P while increasing $E_{\rm F}$. Particularly, in an aligned metallic CNT film, the maximum of P was \sim 5



times larger than that in the highest-purity (>99%) single-chirality semiconducting CNT film. We attribute these superior thermoelectric properties of metallic CNTs to the simultaneously enhanced S and σ of one-dimensional conduction electrons near the first van Hove singularity.

KEYWORDS: thermoelectric, single-wall carbon nanotubes, nanomaterials, ionic liquid, electrical double-layer technique, one dimension

here is an increasing recognition that efficient conversion of waste heat to electrical power is key to the successful development of wearable electronics and photonics. Much recent attention has been paid to nanostructured semiconductor materials, including semiconducting polymers and carbon nanotubes (CNTs), for the development of wearable thermoelectric devices because of their flexibility and scalability in addition to their expected superb thermoelectric properties. Semiconductors have always been preferred for thermoelectric device applications, and little attention has been paid to metals because of their typically small Seebeck coefficient (S).^{2,3}

A maximum S in a semiconductor is achieved when the Fermi energy, $E_{\rm F}$, is shifted from the middle of the band gap, or the charge neutrality point (CNP), by an amount on the order of the thermal energy k_BT . However, at this value of E_F , the carrier density, and hence electrical conductivity σ , is very small; see Figure 1a. When the $E_{\rm F}$ is further moved away from the CNP gradually, increasing the carrier density either on the p- or n-side, σ tends to increase monotonically, but S tends to decrease monotonically. Therefore, the thermoelectric power factor $P = S^2 \sigma$ continuously remains small as one varies the $E_{\rm F}$. This trade-off between S and σ is a well-known dilemma, preventing the development of high-performance thermoelectric devices.

A special case arises in certain 4f-electron metals, which have exhibited unusually large P values. This can be explained as a result of the existence of a narrow 4f-electron peak in density of states (DOS) in the vicinity of E_F , as, in general, the best thermoelectric is expected in materials that have a sharp singularity in DOS very close to E_F. CNTs can embody this scenario if E_F can be precisely tuned to a one-dimensional (1D) van Hove singularity (vHs), as pointed out by Hicks and Dresselhaus.7 Previous experiments have examined the thermoelectric properties of various types of single-wall CNT (SWCNT) samples. $^{8-16}$ Semiconducting SWCNTs have been

Received: July 23, 2019 Revised: September 3, 2019 Published: September 5, 2019

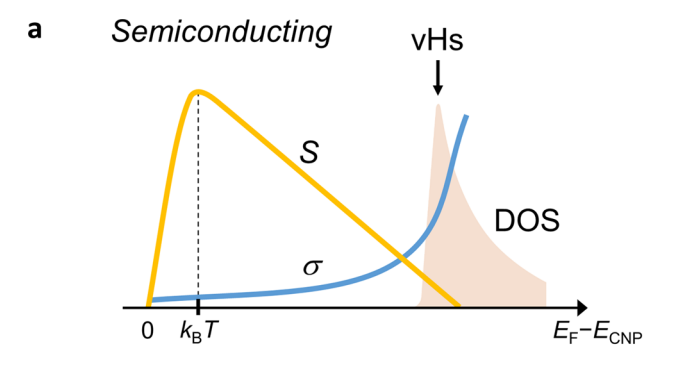
Department of Physics, Tokyo Metropolitan University, Tokyo 192-0372, Japan

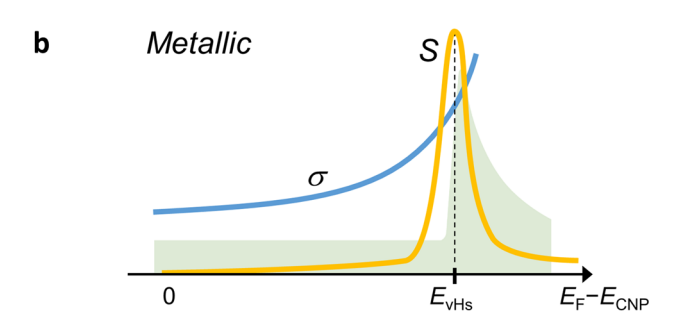
^{*}Department of Electrical and Computer Engineering, Rice University, Houston, Texas 77005, United States

[§]Department of Liberal Arts, Faculty of Engineering, Tokyo University of Science, Katsushika, Tokyo 125-8585, Japan

Department of Physics and Astronomy, Rice University, Houston, Texas 77005, United States

 $^{^\}perp$ Department of Material Science and NanoEngineering, Rice University, Houston, Texas 77005, United States





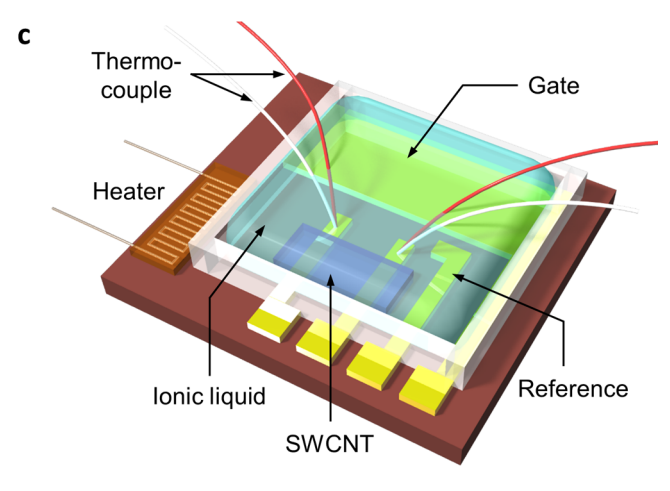


Figure 1. Mechanism of how a Fermi-energy-tuned metallic carbon nanotube can outperform a semiconducting nanotube as a thermo-electric material. The expected behaviors of the Seebeck coefficient (S) and electrical conductivity (σ) of (a) semiconducting and (b) metallic carbon nanotubes as a function of Fermi energy ($E_{\rm F}$) measured from the charge neutrality point ($E_{\rm CNP}$). Note that the thermoelectric power factor is $P=S^2\sigma$, so a high P requires simultaneously large S and σ , which is possible only in metallic nanotubes. (c) Schematic diagram of the experimental setup used for measuring thermoelectric properties of carbon nanotube films using electrolyte gating.

shown to possess a large $S^{.11,14,17-21}$ In contrast, metallic SWCNTs have been largely disregarded in thermoelectric studies because of their typically small S under normal circumstances, 12 and, in fact, a great deal of effort has been expended to remove small amounts of metallic SWCNTs from semiconductor-enriched SWCNT specimens because they degrade thermoelectric properties. 22 However, since metallic SWCNTs also possess vHs in DOS, one should observe thermoelectric enhancement if $E_{\rm F}$ is moved far away from the

charge neutrality point (CNP) and tuned to coincide with a vHs, where the σ is also enhanced; see Figure 1b.

Here, we systematically investigated the $E_{\rm F}$ dependence of $S_{\rm F}$ σ , and P in a variety of films containing high-purity (>99%) single-chirality semiconducting SWCNTs, high-purity metallic SWCNTs, and their mixtures with different content ratios. In all samples, in which metallic nanotubes are present, we observed a nontraditional regime where both S and σ increased with $E_{\rm F}$. Correspondingly, S increased with σ in this regime. This novel regime was followed by a traditionally seen regime, in which S decreased with σ in films consisting of both semiconducting and metallic SWCNTs. However, in purely metallic films, S monotonically increased with σ throughout the entire $E_{\rm F}$ range we covered; namely, the thermoelectric trade-off problem has been solved by the use of purely metallic SWCNT films. Notably, the maximum value of P achieved in an aligned metallic SWCNT film, $\sim 300 \ \mu \text{Wm}^{-1} \text{ K}^{-2}$, was five times larger than that obtained in the highest-purity singlechirality semiconducting SWCNT film.

Table 1 summarizes the main five SWCNT samples we studied in this work (samples 1–5). We first prepared two

Table 1. Five SWCNT Film Samples with Varying Semiconductor—Metal Ratios^a

sample	(6,5) content (%)	metallic content (%)	synthesis and enrichment	aligned?
1	>99	<1	CoMoCAT and GC	no
2	90	10	mixture of 1 and 4	no
3	50	50	mixture of 1 and 4	no
4	<1	>99	arc discharge and DGU	no
5	<1	>96	arc discharge and DGU	yes

"Note that (6,5) single-wall carbon nanotubes are semiconducting with a band gap of ~ 1 eV. Abbreviations: GC = gel chromatography; DGU = density gradient ultracentrifugation.

highly purified SWCNT ensemble samples: samples 1 and 4. Sample 1 was enriched in (6,5) semiconducting SWCNTs, synthesized by the CoMoCAT method, using gel chromatography with precise pH control²³ with a chirality purity over 99%; sample 4 was enriched in metallic SWCNTs with an average diameter of 1.4 nm (metallic purity >99%), synthesized by the arc-discharge method and enriched by density gradient ultracentrifugation.²⁴ More information about sample characteristics and chirality purity evaluation methods can be found in the Supporting Information; see Figures S1 and S2. Furthermore, by mixing samples 1 and 4 at certain ratios, we prepared sample 2, in which the (6,5)-to-metal ratio was 9:1, and sample 3, in which the (6,5)-to-metal ratio was 1:1. Finally, we used the controlled vacuum filtration method^{25,26} to prepare a highly aligned metallic SWCNT film, sample 5. See Figure S5 for the basic characteristics of sample 5. To investigate the thermoelectric properties of these samples as a function of $E_{\rm F}$, we employed the methods of electrolyte gating described previously. Figure 1c shows a schematic illustration of the experimental setup. We injected electrons and holes through electric double-layer formation, which was controlled by the gate voltage, $V_{\rm G}$. The device structure is schematically depicted in Figure S3.

Figure 2 shows experimentally measured values of σ , S, and P for Samples 1–5 as a function of $V_{\rm G}$. In all plots, the CNP is set to be at $V_{\rm G}=0$. Figure 2a shows σ versus $V_{\rm G}$ for the five

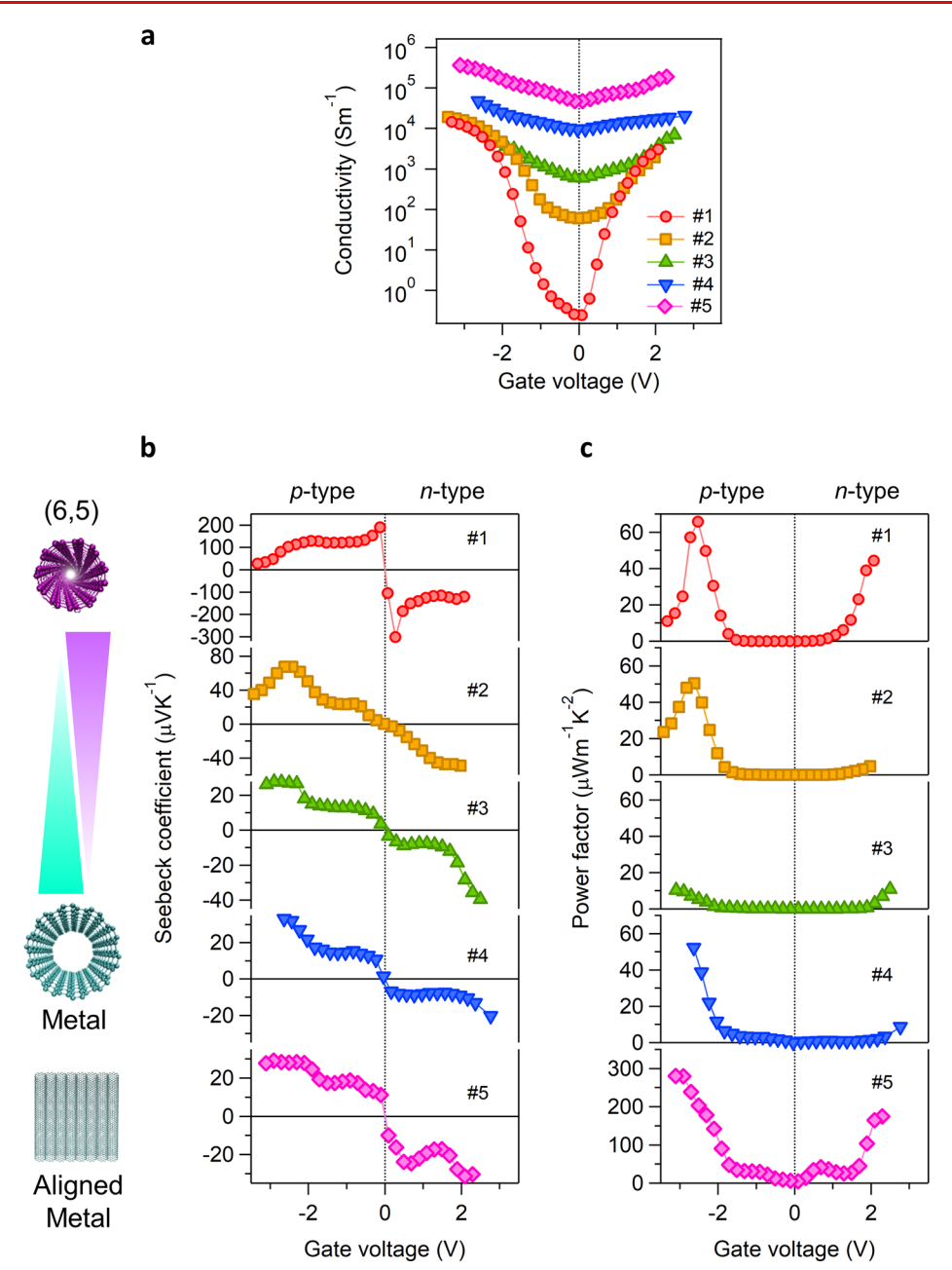


Figure 2. Gate-tuning the thermoelectric properties of semiconductor-enriched, type-mixed, and metal-enriched single-wall carbon nanotubes. (a) Electrical conductivity (σ) , (b) Seebeck coefficient (S), and (c) power factor $(P = S^2\sigma)$ as a function of gate voltage for a series of samples with different semiconductor-metal ratios (sample 1, red circles; sample 2, orange squares; sample 3, green triangles; sample 4, blue inverted triangles; sample 5, pink diamonds). See Table 1 for sample descriptions.

samples; all samples exhibited transistor behavior with on/off ratios varying from $\sim\!10^5$ (sample 1) to <10 (samples 4 and 5). Figure 2b shows S versus $V_{\rm G}$ for the samples, where $E_{\rm F}$ was tuned in a wide range, going from the p-type regime to the n-type regime. In sample 1, positive and negative peaks are observed slightly below and above the CNP, respectively, with a sudden change of sign of S at the CNP. This is a typical behavior for semiconductors, with the peak separation in energy given by $\sim\!\!k_{\rm B}T$. The data for sample 2 in Figure 2b shows that inclusion of metallic SWCNTs, even at 10%, significantly decreases the peak S value from 300 $\mu{\rm VK}^{-1}$ to 60 $\mu{\rm VK}^{-1}$ and, at the same time, drastically changes the overall $V_{\rm G}$ dependence. As the metal content further increases, the peak structure in the $S\!-\!V_{\rm G}$ curve tends to diminish (sample 3), and

in the 100% metallic case (samples 4 and 5), no peak structure is observed.

Figure 2c shows the corresponding $V_{\rm G}$ dependence of the power factor, P, for the five samples, exhibiting sharp peaks. A peak in P is expected to appear when the $E_{\rm F}$ coincides with the first vHs either in the valence or conduction band. The sharpness of the power factor peak for sample 1 indicates that fine-tuning of $V_{\rm G}$ is necessary for achieving and maintaining a high power factor in a highly purified (6,5) SWCNT sample. When the chirality purity is higher, the peak power factor value is higher at the vHs, as demonstrated by the data for Samples 1, 2, and 3 in Figure 2c. However, in sample 4 (>99% metallic) at a high $|V_{\rm G}|$, such as when $V_{\rm G} < -2$ V, it is seen that P continues to increase, reaching the value for the highest-purity

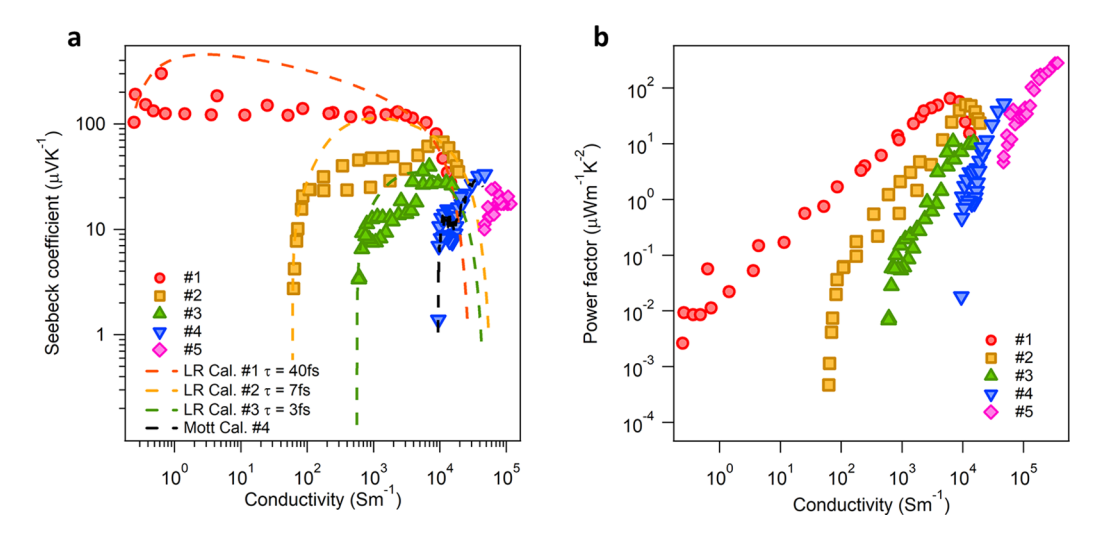


Figure 3. Seebeck coefficient and power factor of carbon nanotube films with different semiconductor-metal ratios. (a) Relationship between Seebeck coefficient and conductivity of the five samples with different semiconductor-metal ratios (see Table 1). (b) Relationship between power factor and conductivity of the five samples (sample 1, red circles; sample 2, square oranges; sample 3, green triangles; sample 4, blue inverted triangles; sample 5, pink diamonds). The dashed lines in part a are theoretical simulations. Mott's formula, eq 1, was used for sample 4 (Mott Cal.), whereas the linear response theory combined with the thermal Green's function method within the constant-relaxation-time approximation was used for samples 1–3 (LR Cal.).

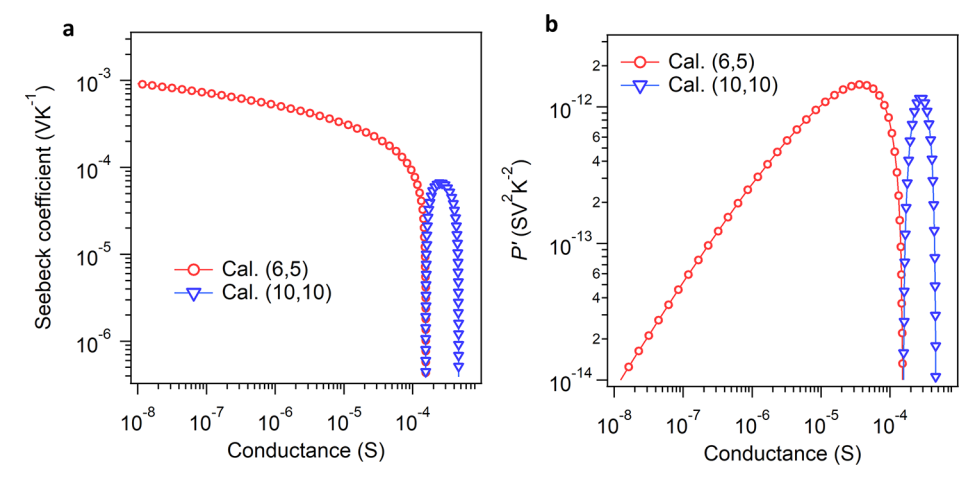


Figure 4. Calculated Seebeck coefficient and power factor of (6,5) and (10,10) SWCNTs as a function of electrical conductance. (a) Relationship between Seebeck coefficient and electrical conductance and (b) relationship between power factor and electrical conductance for a (6,5) SWCNT (red circles) and a (10,10) SWCNT (blue triangles) calculated using the nonequilibrium Green's function method.

semiconducting sample (sample 1). Finally, the peak *P* value of an aligned metallic film (sample 5) exceeds that of sample 1.

Figure 3a is a summary of the relationship between S and σ for the five samples. This figure highlights the following three points: (1) In the metallically purified SWCNT samples (samples 4 and 5), S increases monotonically with σ , i.e., the trade-off between them is fully eliminated. (2) As the content of semiconducting species increases (samples 2 and 3), the range where the trade-off is lifted becomes narrower and shifts toward a lower σ region, and a plateau region develops. (3) In the highest-purity semiconducting sample (sample 1), the unconventional regime is absent, i.e., S decreases with increasing σ in the entire range.

In the highest conductivity region, $\sigma > 10^4~{\rm Sm}^{-1}$, only the *S* of the purely metallic samples continues to increase, while those of the other samples rapidly decrease with increasing σ . The same behavior is also seen in the power factor, *P*, as shown in Figure 3b. Sample 1 exhibits a peak at $\sigma \sim 6 \times 10^3~{\rm Sm}^{-1}$, while samples 2 and 3 show peaks at $\sigma \sim 1 \times 10^4~{\rm Sm}^{-1}$.

Samples 4 and 5 show a continuous increase of P with σ up to the highest value of σ . The highest value of P of sample 4 (achieved at the highest σ) is essentially equal to that of sample 1 (achieved at $\sigma \sim 6 \times 10^3 \ \mathrm{Sm^{-1}}$) within the experimental error. Sample 5 exhibits an even higher P than sample 4, as expected from the fact that alignment leads to an enhanced σ , while S remains constant. The highest value of P of sample 5 is $\sim 300 \ \mu\mathrm{Wm^{-1}\ K^{-2}}$, which is the highest among all the samples studied. That is, the aligned and metallically enriched SWCNT film outperforms the highest-purity semiconducting SCWNT film in terms of thermoelectric power factor.

To understand these observations more quantitatively, we first analyzed the relationship between S and σ for sample 4 using the standard Mott formula for metals:²⁹

$$S = -\frac{\pi^2 k_{\rm B}^2 T}{3e} \frac{1}{\sigma(V_{\rm G})} \frac{\partial \sigma}{\partial V_{\rm G}} \left(\frac{\partial E_{\rm F}}{\partial V_{\rm G}} \right)^{-1} \tag{1}$$

Here, $\sigma(V_{\rm G})$ is the experimentally measured $V_{\rm G}$ -dependent σ . We assume $\partial E_{\rm F}/\partial V_{\rm G}$ to be constant; that is, $E_{\rm F}=\alpha V_{\rm G}$, where α is a fitting parameter. This procedure reproduced the experimental data for sample 4 well (see Figure 3a), indicating that, in metallic SWCNTs, the behavior is consistent with the conventional Mott formula, in which the increase of S can be attributed to the increase of DOS as $E_{\rm F}$ increases. Hence, the simultaneous increase of S and S can be interpreted as a consequence of the S approaching the first 1D vHs in metallic SWCNTs.

However, high-purity semiconducting samples (samples 1 and 2) cannot be explained within the conventional Mott formalism (see Figure S4). Equation 1, or an approximate formula more appropriate for conventional semiconductors, 1,2 completely fails to reproduce the observed behavior. Therefore, in order to calculate the relationship between S and σ in samples 1-3, we used the linear response theory combined with the thermal Green's function method within the constantrelaxation-time approximation.¹⁷ The details of the calculation procedure are given in the Supporting Information. We assumed that the electronic dispersions near the conductionand valence-band edges of a (6,5) SWCNT can be described as gapped 1D Dirac bands. The presence of metallic SWCNT impurities in these samples can be treated by introducing finite DOS inside the band gap, or "in-gap states," the amount of which can be represented by the relaxation time of Dirac electrons. The calculation results are shown as dashed lines in Figure 3a. There is a good overall agreement between theory and experiment.

To further corroborate our finding that metallic SWCNTs can be better thermoelectric materials than semiconducting SWCNTs, we examined the relationships among S, electrical conductance (G), and $P' \equiv S^2G$ of single (6,5) and (10,10) SWCNTs using the nonequilibrium Green's function formalism (Figure 4). Detailed calculation methods are given in the Supporting Information. As shown in Figure 4a, for a (6,5) SWCNT, which is semiconducting, S decreases as G increases; i.e., the usual trade-off is observed. However, in a (10,10) SWCNT, which is metallic, we can identify a region where S and G simultaneously increase, which is similar to the experimentally observed behavior. These calculations clearly indicate that this behavior is caused by the enhancement of S around the first vHs of the metallic SWCNT; see also Figure S6 and a previous study. 20 Regarding the power factor (Figure 4b), in a large G region (> 10^{-4} S), the P' of the (10,10) SWCNT increases with G, achieving a peak value at $G \approx 2 \times$ 10^{-4} S, which is comparable to the peak P' value of the (6,5) SWCNT. Although these calculations were performed on single SWCNTs and thus cannot be directly compared with our experimental data on macroscopic films, the results basically support the notion that a Fermi-energy-optimized metallic SWCNT can be a better thermoelectric material than a semiconducting SWCNT.

It is important to emphasize that metallic SWCNTs show negligibly small S and P when $E_{\rm F}$ is near the CNP, consistent with conventional wisdom that high-purity semiconducting nanomaterials are far superior to metallic nanomaterials for thermoelectric applications. However, metallic SWCNTs are unique in possessing semiconductor-like properties, 30,31 especially wide Fermi-energy tunability. When we move $E_{\rm F}$ from the CNP, either to the p- or n-side, both S and σ increase. This behavior can be attributed to the existence of the 1D vHs in the DOS of metallic SWCNTs. Contrastingly, although

there is a plateau region where S is almost constant as a function of σ , semiconducting SWCNTs exhibit the conventional trade-off, i.e., S decreases with increasing σ . As a result, the P of metallic SWCNTs can become larger than that of semiconducting SWCNTs in the largest σ region.

Methods. *SWCNT Film Preparation*. A high-purity ensemble of (6,5) SWCNTs (sample 1) was prepared through gel chromatography from the original SWCNTs synthesized by the CoMoCAT method (SG65, Sigma-Aldrich). Details of this separation procedure can be found in ref 23. Metallic SWCNTs (sample 4) were prepared using density gradient ultracentrifugation from the original SWCNTs synthesized by the arc-discharge method (Arc SO, Meijyo Nano Carbon Co.). The SWCNT concentrations of samples 1 and 4 were adjusted so that the absorbance at the first vHs becomes the same level. Samples 2 and 3 were prepared by mixing samples 1 and 4 at the volume ratios indicated in Table 1. Each sample was poured into the funnel of a vacuum filtration system and filtered through a PTFE membrane (Omnipore 0.2 µm PTFE Membrane, Merck Millipore Ltd.), and surfactants on SWCNTs such as sodium deoxycholate (DOC) or iodixanol were replaced by Triton (polyoxyethylene octylphenyl ether, Wako pure chemical Industries, Ltd.). Subsequently, the SWCNTs in the redispersed solution were filtered through a polycarbonate membrane filter (Whatman Nuclepore Track-Etched membrane 25 mm 0.2 μ m) to form a thin film.

Aligned Metallic SWCNT Film (Sample 5) Preparation. Metallic SWCNTs were separated by density gradient ultracentrifugation in the same manner as sample 4. We then conducted ultrafiltration (Amicon Ultra-15 Centrifugal Filters Ultracel, 100 K, Merck Millipore Ltd.) on the resulting metallically enriched solution to exchange the solvent from DOC/iodixanol to 0.3% DOC. Subsequently, the obtained suspension was sonicated with a tip sonicator (XL-2000 Sonicator, Qsonica, 1/4 in. probe, ~30 W) for 5-10 min and centrifuged for 15-20 min at 38 000 rpm (Beckman-Coulter Optima L-80 XP Preparatory Ultracentrifuge (BSI414) using a Beckman SW-41 Ti swing bucket rotor). The upper 80% of the SWCNT suspension in the centrifuge tube was collected and then diluted with pure water to have a surfactant concentration of 0.013% DOC. The suspension was then poured into the funnel of a vacuum filtration system and slowly filtered through a polycarbonate membrane filter (Whatman Nuclepore Track-Etched membrane 25 mm 0.2 μ m) under well-controlled conditions to form an aligned SWCNT film. See Figure S5 for more information on the sample preparation methods and characteristics of sample 5.

Device Preparation. The prepared SWCNT thin film was transferred onto a polyimide/parylene substrate with predeposited gold electrodes (thickness ~ 100 nm). Residual polymers such as polycarbonate or polyvinylpyrrolidone were dissolved and washed by chloroform and acetone. The length, width, and thickness of the film were respectively $\sim 600 \mu m$, \sim 1 mm, and \sim 80 nm. To remove residual Triton and organic solvent, the sample was annealed at 200 °C for 2 h in a vacuum (<10⁻³ Pa). A heater (KFR-02N-120-C1-11N10C2, Kyowa Dengyo Co.) was attached on one side of the film, and thermocouples (KFT(TW)-50-100-050, ANBE SMT Co.) were fixed on the electrodes at both film ends by silver paste (D-500 DOTITE, Fujikura Kasei Co.). To make sure that no chemical reaction occurs between silver and ionic liquid, insulating sealant (TSE397-C, Momentive Performance Materials Japan LLC.) covered the silver paste. Ionic liquid

(TMPA-TFSI, Kanto Chemical Co.) was dropped to cover the SWCNT film and gate electrodes to create an electrolyte gating system.

Conductivity and Seebeck Coefficient Measurements. Electrical conductivity and Seebeck coefficient measurements were conducted in a vacuum ($\sim 10^{-3}$ Pa) using a vacuum and low-temperature probe station (Grail 10, Nagase Techno Co.). By changing the gate voltage from +3.2 V to -2.8 V, we injected electrons or holes into the SWCNT film, shifting the $E_{\rm E}$. For the transport measurements, the source-drain voltage was kept as small as possible, such as 0.1 V for (6,5) and 5 mV for metallic SWCNTs, and then the transport properties were evaluated in the linear response region. The conductivity was calculated from the measured resistance of the film at each gate voltage. The Seebeck coefficient as a function of gate voltage was measured in the same manner as that described in ref 11. The Seebeck coefficients were always measured in the same gate-shift direction, such as from positive to negative, in order to eliminate the influence of hysteresis during the measure-

Theoretical Calculations. The details of theoretical calculations based on the linear response theory combined with the thermal Green's function method within the constant-relaxation-time approximation, and the details of calculated power factor of single (6,5) and (10, 10) SWCNTs are described in the Supporting Information.

ASSOCIATED CONTENT

S Supporting Information

The Supporting Information is available free of charge on the ACS Publications website at DOI: 10.1021/acs.nanolett.9b03022.

Sample information, purity evaluation for the high-purity (6,5) sample, device pictures, comparison between experimental data and theoretical calculations by the Mott formula for samples 1–4, information on the aligned metallic SWCNT film, details of theoretical calculations based on the linear response theory combined with the thermal Green's function method within the constant-relaxation-time approximation, details of the theoretical calculation on thermoelectric properties of single (6,5) and (10,10) SWCNTs, calculated conductance, Seebeck coefficient, power factor, and DOS of (6,5) and (10,10) SWCNTs (PDF)

AUTHOR INFORMATION

Corresponding Authors

*E-mail: kono@rice.edu. Phone: +1-713-348-2209.

*E-mail: yanagi-kazuhiro@tmu.ac.jp. Phone: +81-42-677-2494.

ORCID

Yohei Yomogida: 0000-0002-8569-6179 Junichiro Kono: 0000-0002-4195-0577 Kazuhiro Yanagi: 0000-0002-7609-1493

Author Contributions

K.Y., J.K., W.G., and Y.Y. led this study. Y.I., A.Y., K.H., K.F., and N.K. carried out the experiments. M.M. and T.Y. performed the theoretical calculations. All authors discussed the results and contributed to the writing of the manuscript.

Notes

The authors declare no competing financial interest.

ACKNOWLEDGMENTS

We thank Hidetoshi Fukuyama for valuable discussions. K.Y. acknowledges support by JSPS KAKENHI through Grant Numbers JP17H06124, JP17H01069, and JP18H01816 and JST CREST through Grant Number JPMJCR17IS, Japan. J.K. acknowledges support from the U.S. Department of Energy Basic Energy Sciences through Grant Number DEFG02-06ER46308 (optical spectroscopy), the U.S. National Science Foundation through Grant Number ECCS-1708315 (device fabrication), and the Robert A. Welch Foundation through Grant Number C-1509 (sample preparation). T.Y. acknowledges support by JSPS KAKENHI through Grant Number JP18H01816. Y.I. acknowledges support by JSPS KAKENHI through Grant Number JP19J21142.

ABBREVIATIONS

CNTs, carbon nanotubes; CNP, charge neutrality point; DOS, density of states; 1D, one-dimensional; vHs, van Hove singularity; SWCNT, single-wall carbon nanotube

REFERENCES

- (1) Bahk, J.-H.; Fang, H.; Yazawa, K.; Shakouri, A. Flexible Thermoelectric Materials and Device Optimization for Wearable Energy Harvesting. *J. Mater. Chem. C* **2015**, *3*, 10362–10374.
- (2) Smith, R. A. Semiconductors; Cambridge University Press: Cambrige, 1959.
- (3) Aschcroft, N. W.; Mermin, N. D. Solid State Physics; Saunders College: Philadelphia, 1976.
- (4) Rowe, D. M.; Min, G. α -ln σ Plot as a Thermoelectric Material Performance Indicator. *J. Mater. Sci. Lett.* **1995**, *14*, 617–619.
- (5) van Daal, H. J.; van Aken, P. B.; Buschow, K. H. J. The Seebeck Coefficient of Ybal₂ and Ybal₃. *Phys. Lett. A* **1974**, *49*, 246–248.
- (6) Mahan, G. D.; Sofo, J. O. The Best Thermoelectric. *Proc. Natl. Acad. Sci. U. S. A.* **1996**, 93, 7436–7439.
- (7) Hicks, L. D.; Dresselhaus, M. S. Thermoelectric Figure of Merit of a One-Dimensional Conductor. *Phys. Rev. B: Condens. Matter Mater. Phys.* **1993**, 47, 16631–16634.
- (8) Small, J. P.; Perez, K. M.; Kim, P. Modulation of Thermoelectric Power of Individual Carbon Nanotubes. *Phys. Rev. Lett.* **2003**, *91*, 256801.
- (9) Llaguno, M. C.; Fischer, J. E.; Johnson, A. T.; Hone, J. Observation of Thermopower Oscillations in the Coulomb Blockade Regime in a Semiconducting Carbon Nanotube. *Nano Lett.* **2004**, *4*, 45–49.
- (10) Nonoguchi, Y.; Ohashi, K.; Kanazawa, R.; Ashiba, K.; Hata, K.; Nakagawa, T.; Adachi, C.; Tanase, T.; Kawai, T. Systematic Conversion of Single Walled Carbon Nanotubes into N-Type Thermoelectric Materials by Molecular Dopants. *Sci. Rep.* **2013**, *3*, 3344.
- (11) Yanagi, K.; Kanda, S.; Oshima, Y.; Kitamura, Y.; Kawai, H.; Yamamoto, T.; Takenobu, T.; Nakai, Y.; Maniwa, Y. Tuning of the Thermoelectric Properties of One-Dimensional Material Networks by Electric Double Layer Techniques Using Ionic Liquids. *Nano Lett.* **2014**, *14*, 6437–6442.
- (12) Nakai, Y.; Honda, K.; Yanagi, K.; Kataura, H.; Kato, T.; Yamamoto, T.; Maniwa, Y. Giant Seebeck Coefficient in Semi-conducting Single-Wall Carbon Nanotube Film. *Appl. Phys. Express* **2014**, *7*, 025103.
- (13) Fukumaru, T.; Fujigaya, T.; Nakashima, N. Development of *N*-Type Cobaltocene-Encapsulated Carbon Nanotubes with Remarkable Thermoelectric Property. *Sci. Rep.* **2015**, *5*, 7951.
- (14) Avery, A. D.; Zhou, B. H.; Lee, J.; Lee, E.; Miller, E. M.; Ihly, R.; Wesenberg, D.; Mistry, K. S.; Guillot, S. L.; Zink, B. L.; et al.

Tailored Semiconducting Carbon Nanotube Networks with Enhanced Thermoelectric Properties. *Nat. Energy* **2016**, *1*, 16033.

- (15) Shimizu, S.; Iizuka, T.; Kanahashi, K.; Pu, J.; Yanagi, K.; Takenobu, T.; Iwasa, Y. Thermoelectric Detection of Multi-Subband Density of States in Semiconducting and Metallic Single-Walled Carbon Nanotubes. *Small* **2016**, *12*, 3388–3392.
- (16) Zhou, W.; Fan, Q.; Zhang, Q.; Cai, L.; Li, K.; Gu, X.; Yang, F.; Zhang, N.; Wang, Y.; Liu, H.; et al. High-Performance and Compact-Designed Flexible Thermoelectric Modules Enabled by a Reticulate Carbon Nanotube Architecture. *Nat. Commun.* **2017**, *8*, 14886.
- (17) Yamamoto, T.; Fukuyama, H. Bipolar Thermoelectric Effects in Semiconducting Carbon Nanotubes: Description in Terms of One-Dimensional Dirac Electrons. *J. Phys. Soc. Jpn.* **2018**, *87*, 114710.
- (18) Norton-Baker, B.; Ihly, R.; Gould, I. E.; Avery, A. D.; Owczarczyk, Z. R.; Ferguson, A. J.; Blackburn, J. L. Polymer-Free Carbon Nanotube Thermoelectrics with Improved Charge Carrier Transport and Power Factor. ACS Energy Lett. 2016, 1, 1212–1220.
- (19) Hung, N. T.; Nugraha, A. R. T.; Hasdeo, E. H.; Dresselhaus, M. S.; Saito, R. Diameter Dependence of Thermoelectric Power of Semiconducting Carbon Nanotubes. *Phys. Rev. B: Condens. Matter Mater. Phys.* **2015**, 92, 165426.
- (20) Jiang, J.; Wang, J.; Li, B. A Nonequilibrium Green's Function Study of Thermoelectric Properties in Single-Walled Carbon Nanotubes. *J. Appl. Phys.* **2011**, *109*, 014326.
- (21) Yamamoto, T.; Fukuyama, H. Possible High Thermoelectric Power in Semiconducting Carbon Nanotubes ~ a Case Study of Doped One-Dimensional Semiconductors~. *J. Phys. Soc. Jpn.* **2018**, 87, 024707.
- (22) Hayashi, D.; Ueda, T.; Nakai, Y.; Kyakuno, H.; Miyata, Y.; Yamamoto, T.; Saito, T.; Hata, K.; Maniwa, Y. Thermoelectric Properties of Single-Wall Carbon Nanotube Films: Effects of Diameter and Wet Environment. *Appl. Phys. Express* **2016**, *9*, 025102.
- (23) Ichinose, Y.; Eda, J.; Yomogida, Y.; Liu, Z.; Yanagi, K. Extraction of High-Purity Single-Chirality Single-Walled Carbon Nanotubes through Precise Ph Control Using Carbon Dioxide Bubbling. J. Phys. Chem. C 2017, 121, 13391–13395.
- (24) Arnold, M. S.; Green, A. A.; Hulvat, J. F.; Stupp, S. I.; Hersam, M. C. Sorting Carbon Nanotubes by Electronic Structure Using Density Differentiation. *Nat. Nanotechnol.* **2006**, *1*, 60–65.
- (25) He, X.; Gao, W.; Xie, L.; Li, B.; Zhang, Q.; Lei, S.; Robinson, J. M.; Hároz, E. H.; Doorn, S. K.; Wang, W.; et al. Wafer-Scale Monodomain Films of Spontaneously Aligned Single-Walled Carbon Nanotubes. *Nat. Nanotechnol.* **2016**, *11*, 633–638.
- (26) Gao, W.; Kono, J. Science and Applications of Wafer-Scale Crystalline Carbon Nanotube Films Prepared through Controlled Vacuum Filtration. R. Soc. Open Sci. 2019, 6, 181605.
- (27) Oshima, Y.; Kitamura, Y.; Maniwa, Y.; Yanagi, K. Fabrication of Thermoelectric Devices Using Precisely Fermi Level-Tuned Semiconducting Single-Wall Carbon Nanotubes. *Appl. Phys. Lett.* **2015**, *107*, 043106.
- (28) Fukuhara, K.; Ichinose, Y.; Nishidome, H.; Yomogida, Y.; Katsutani, F.; Komatsu, N.; Gao, W.; Kono, J.; Yanagi, K. Isotropic Seebeck Coefficient of Aligned Single-Wall Carbon Nanotube Films. *Appl. Phys. Lett.* **2018**, *113*, 243105.
- (29) Cutler, M.; Mott, N. F. Observation of Anderson Localization in an Electron Gas. *Phys. Rev.* **1969**, *181*, 1336–1340.
- (30) Haroz, E. H.; Duque, J. G.; Lu, B. Y.; Nikolaev, P.; Arepalli, S.; Hauge, R. H.; Doorn, S. K.; Kono, J. Unique Origin of Colors of Armchair Carbon Nanotubes. *J. Am. Chem. Soc.* **2012**, *134*, 4461–4464.
- (31) Hároz, E. H.; Duque, J. G.; Tu, X.; Zheng, M.; Hight Walker, A. R.; Hauge, R. H.; Doorn, S. K.; Kono, J. Fundamental Optical Processes in Armchair Carbon Nanotubes. *Nanoscale* **2013**, *5*, 1411–1439.